Homotopy Perturbation Method For Heat Transfer Of Peristaltic Flow Of Viscoelastic Fluid In Eccentric Cylinder With Varaible Effects

Tagreed Alarabi[1], Assma F. Elsayed[2] and O Anwar Bég[3^]

[1]Math. Dept., Faculty of applied science, Tibah University, Almadinah Al Monwara, Saudi Arabia
[2]Math Dept. Faculty of Education, Ain shams, University, Heliopolis, Cairo, Egypt. assma_elsayed@yahoo.com
[3]Department of Engineering and Mathematics, Sheffield Hallam University, UK
gortoab@gmail.com

Abstract: In this paper the Homotopy perturbation method **(HPM)** has been used to solve the normalized system of non-linear partial differential equations describing the momentum, energy and mass transfer, under appropriate boundary conditions of peristaltic viscoelastic Jeffery fluid flow with complaint wall. The influence of Prandtl number, Eckert number, radius, time, on variable viscosity, velocity, temperature and axial pressure gradient distributions are studied graphically.

1. Introduction

Biophysical fluid dynamics constitutes a rich area of modern research in biomechanical engineering. In particular *non-Newtonian transport phenomena* in the human body [1] continue to stimulate the attention of engineering scientists, numerical analysts, applied physicists and mathematical biologists. The strong nonlinearity of flows encountered in non-Newtonian dynamics generally requires powerful numerical methods for robust and pragmatic solutions [2]. Biorheological flows [3] are exemplified by bile, blood, mucus, digestive fluids, synovial lubricants etc [4]. These fluids deviate from the classical Newtonian linear relationship between the shear stress and shear rate. Rheological characteristics exhibited by such fluids are extremely diverse and to address realistic flows, a wide spectrum of non-Newtonian models have been developed over the past five decades. These include micro-structural fluids [5] which mimick rotary motions of particulate suspensions and erythrocytes and are based on Eringen's micro-morphic theory [6]. Viscoelastic fluids [7] offer a different formulation for rheological effects and are aimed at simulating memory effects, tensile stress relaxation, elasticity and other features of real biological liquids. Examples of such models as implemented in medical engineering include the Kelvin-Voigt model [8] in synovial flows, Maxwell's model [9] in blood flows, empirical models [10] for eye fluid dynamics and Oldroyd-B models for embryological transport [11].

In recent years *peristaltic transport* has also garnered significant attention. Peristalsis is a natural mechanism in biology used to pump liquids by means of moving contraction on the tubes or channel walls. It arises in food migration via the esophagus, chyme motion in the gastrointestinal tract, vasomotion of small blood vessels such as venules, capillaries, and arterioles and furthermore, is fundamental to uretral transport from the kidneys to the bladder. Non-Newtonian studies of peristalsis have thrived in recent years. A diverse array of rheological models have been implemented in peristaltic transport including Maxwell fluids [12], Jeffreys fluids [13], Williamson fluids [14], Oldroyd-B fluids [15], Johnson-Segalman fluids [16], nanofluids [17], liquid crystal nematogens [18], couple stress fluids [19] and viscoplastic (Bingham) yield stress fluids [20]. All these models involve a tremendous range of constitutive equations and mimick extensive features arising in actual rheological fluids.

In the vast majority of simulations of non-Newtonian peristaltic flows, the fluid properties such as viscosity are assumed to be constant. In general the coefficients of viscosity for real fluids are functions of space coordinate, temperature, and pressure. An example of a biological problem involving variable viscosity and fluid-structure interaction is the behavior of red blood cells in capillaries. Red blood cells, which have an interior viscosity approximately 5 times greater than the surrounding blood plasma, are known to undergo large deformations as they squeeze through vessels that can be as little as half their diameter. The variation of viscosity due to space coordinate and temperature change is more dominant than other effects. Therefore, it is highly desirable to include the effect of variable viscosity instead of considering the viscosity of the fluid to be constant. Several researchers have considered variable viscosity in peristaltic fluid

dynamics including Tripathi *et al.* [21] who used an exponential model. Further studies include [22]-[30].

Most investigations of peristaltic transport also consider straight conduits and neglect curvature, which is a key feature in actual medical applications. The influence of curvature can be very prominent on flow rates and wave propagation. Interesting studies in this regard have been communicated by Stavitsky *et al.* [31] using a finite element code and Rath [32] who used perturbation methods to solve the inertia-free Navier-Stokes equations. More recently rheological studies of curved tube peristaltic transport have received some attention. Relevant works in this regard include Hina *et al.* [33] who used the Ostwald-deWaele shear thinning model, Hina *et al.* [34] who employed a Johnson-Segalman viscoelastic model, Ali *et al.* [35] who utilized a Reiner-Rivlin third order model and Ali *et al* [36] who implemented the Eringen micropolar model in curved tube rhythmic wall flows.

In recent years many diverse numerical methods have been implemented to analyze complex peristaltic flows. These include finite element codes such as ADINA-FSI [37], COSMOS [38], spectral finite elements [39], variational finite elements [40], upwinding non-iterative finite element analysis [41], Adomian's decomposition method (ADM) [42], Lattice Boltzmann methods (LBM) [43] and finite volume computational fluid dynamics [44]. In recent years the so-called homotopy semi-numerical methods have also emerged as a significant tool in biofluid mechanics and other areas. One particular method, He's homotopy perturbation method (**HPM**) [45], which is a special case of Liao's homotopy analysis method (**HAM**) [46], has proved immensely popular and successful in resolving highly nonlinear biological transport problems. It has recently been implemented in laser bioheat transfer by El Sayed [47] and in peristaltic viscoelastic flow in permeable materials by Tripathi and Bég [48]. The convergence of homotopy perturbation method (**HPM**) has been investigated by Biazar and Ghazvini [49].

In the present study we examine the peristaltic flow of a Jefferys viscoelastic fluid through a eccentric cylindrical conduit with complaint walls in the presence of heat transfer effects. Thermal diffusion and thermal conductivity are considered to be functions of concentration and fluid temperature and furthermore a temperature-dependent viscosity is utilized in the model. Viscous heating effects are also incorporated in the present simulations. The non-linear, non-dimensionalized partial differential equations subject to physically realistic boundary conditions are solved by means of He's Homotopy Perturbation Method (**HPM**). The effects of the physical parameters on the thermal conductivity and fluid temperature have been

sketched graphically. The present study is relevant to novel peristaltic pump designs.

2. Mathematical Transport Model

Let us consider the peristaltic flow of a viscoelastic Jefferys fluid with variable physical properties (fluid viscosity, thermal conductivity and mass diffusivity) through uniform coaxial tubes. The inner tube is taken as a rigid and the outer deformable tube has a sinusoidal wave travelling down its wall. The inner tube is located at the position $r = \delta, z = 0$ as shown in **Fig.1**.
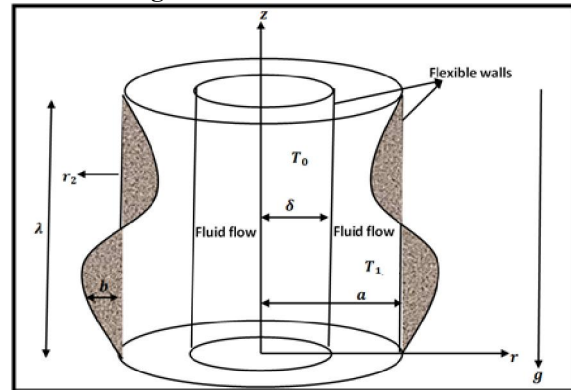

Figure (1). Geometry of the flow and co-ordinate system

We select a cylindrical coordinate system with (r, θ, z) denoting radial, azimuthal and axial coordinates, respectively. The geometrical shapes of the two walls are defined mathematically by the relations:

$$r_1 = \delta, \tag{1}$$

$$r_2 = a + b\,Cos[\frac{2\pi}{\lambda}(z - ct)], \tag{2}$$

Where δ and a are the radii of the inner and outer tubes, b is a amplitude of the wave, λ is the wave length, c is the propagation velocity and t is the time. Further, we assume that the boundary of the inner tube is at the temperature $T_\circ$ and the outer tube is maintained at temperature T_1. If $\overline{V} = (u, v, w)$ is the velocity. The fluid properties are assumed to isotropic and constant, except for the fluid viscosity, thermal conductivity. The continuity, momentum, energy and concentration equations for an incompressible Jeffery fluid are described as follow;

$$\nabla \bullet \overline{V} = 0, \tag{3}$$

$$\rho(\frac{\partial \overline{V}}{\partial t} + \overline{V} \bullet \nabla \overline{V}) = -\nabla p + \nabla \bullet \overline{S} + \rho g \beta_T (T - T_\circ), \tag{4}$$

$$\rho c_p \left(\frac{\partial T}{\partial t} + \overline{V} \bullet \nabla T \right) = \nabla \bullet (k \nabla T) + \overline{S} \bullet \nabla \overline{V}, \tag{5}$$

Where ρ is the density, β_T is the coefficient of thermal expansion. T is the temperature and k is the thermal diffusivity, K_T is the thermal diffusion ratio and $\overline{S}$ for Jeffery fluid is given by the relation

$$\overline{S} = \frac{\mu(T)}{1+\lambda_1}(\gamma^{\bullet} + \lambda_2 \gamma^{\bullet\bullet}), \qquad (6)$$

λ_1 the ratio of relaxation to retardation times, $\gamma^{\bullet}$ the retardation time, $\gamma^{\bullet\bullet} = d\gamma^{\bullet}/dt$ is shear rate, d/dt and λ_2 the material time differentiation. The peristaltic flow of Jeffery fluid is transported by a progressive wave of area contraction or expansion along a complaint wall, the equation corresponding to the compliant wall is [16]

$$L(r_i) = p - p_{\circ} \qquad (7)$$

Where $L = -\tau \dfrac{\partial^2}{\partial z^2} + M_1 \dfrac{\partial^2}{\partial t^2} + d \dfrac{\partial}{\partial t}$ is an operator

.Here, τ is the elastic tension in the membrane, M_1 is the mass per unit area, d is the coefficient of viscous damping and $p_{\circ}$ is the pressure on the outside surface of the wall. It is assumed that $p_{\circ} = 0$ and the walls of the channel are inextensible so that only their lateral motion takes place and the horizontal displacement of the wall is zero Thus the no-slip boundary condition for the velocities is

$$\left.\begin{array}{l} w = 0, \quad T = T_0 \quad , \qquad at \quad r = r_1 \\ T = T_1 \quad , \qquad\qquad\quad at \quad r = r_2 \\ -\tau \dfrac{\partial^3 \eta}{\partial z^3} + M_1 \dfrac{\partial^3 \eta}{\partial z \partial t^2} + d \dfrac{\partial^2 \eta}{\partial z \partial t} = -\rho\left(\dfrac{\partial w}{\partial t} + \overline{V} \bullet \nabla w\right) + \nabla \bullet \overline{S} \\ \quad + \rho g \beta_T (T - T_{\circ}) \quad at \quad \eta = r = r_i, i = 1,2 \end{array}\right\} (8)$$

let us assume that the velocity field for the flow is $\overline{V} = (u,0,w)$. The dimensionless parameters used in the problem are defined as follows

$$\left.\begin{array}{l} z^* = \dfrac{z}{\lambda}, \quad r^* = \dfrac{r}{a}, \quad u^* = \dfrac{\lambda}{ac}u, \quad w^* = \dfrac{w}{c}, \quad \delta^* = \dfrac{\delta}{a}, \quad p^* = \dfrac{a^2}{\mu_{\circ}c\lambda}p, \\ r_1^* = \dfrac{r_1}{a}, t^* = \dfrac{c}{\lambda}t, \phi = \dfrac{b}{a}, \varepsilon^* = \dfrac{\varepsilon}{a}, \quad \overline{S}^* = \dfrac{a}{\mu_{\circ}c}\overline{S}, \quad T^* = \dfrac{T-T_1}{T_{\circ}-T_1}, \\ r_2^* = \dfrac{r_2}{a}, \mu^*(T^*) = \dfrac{\mu(T)}{\mu_0}, K^*(T^*) = \dfrac{k(T)}{k_{\circ}}, R_e = \dfrac{ca\rho}{\mu_{\circ}}, \delta_{\circ} = \dfrac{a}{\lambda}, \end{array}\right\}(9)$$

Where ϕ is the amplitude ratio, $\delta_{\circ}$ is the dimensionless wave number. Using the above dimensionless parameters, the governing equations are reduced to the following form after dropping star mark

$$\frac{\partial u}{\partial r} + \frac{u}{r} + \frac{\partial w}{\partial z} = 0, \qquad (10)$$

$$R_e \delta_{\circ}^3 \left(\frac{\partial u}{\partial t} + u\frac{\partial u}{\partial r} + w\frac{\partial u}{\partial z}\right) = -\frac{\partial p}{\partial r} + \delta_{\circ}\left(\left(\frac{1}{r}\frac{\partial}{\partial r}(rS_{rr})\right) + \delta_{\circ}\frac{\partial S_{rz}}{\partial z} - \frac{S_{\theta\theta}}{r}\right) (11)$$

$$R_e \delta_{\circ}\left(\frac{\partial w}{\partial t} + u\frac{\partial w}{\partial r} + w\frac{\partial w}{\partial z}\right) = -\frac{\partial p}{\partial z} + \frac{1}{r}\frac{\partial}{\partial r}(rS_{rz}) + \delta_{\circ}\frac{\partial S_{zz}}{\partial z} + G_r T, \qquad (12)$$

$$P_r R_e \delta_{\circ}\left(\frac{\partial T}{\partial t} + u\frac{\partial T}{\partial r} + w\frac{\partial T}{\partial z}\right) = \frac{1}{r}\left(K(T)r\frac{\partial T}{\partial r}\right) + \delta_{\circ}^2\frac{\partial}{\partial z}\left(k(T)\frac{\partial T}{\partial z}\right) + P_r E_c \delta_{\circ}$$

$$\left(S_{rr}\frac{\partial u}{\partial r} + \frac{S_{rz}}{\delta_{\circ}}\frac{\partial w}{\partial r} + \delta_{\circ}S_{rz}\frac{\partial u}{\partial z} + S_{zz}\frac{\partial w}{\partial z}\right), \qquad (13)$$

The dimensionless boundary conditions are

$$\left.\begin{array}{l} w = 0, \qquad T = 0 \qquad at \quad r = r_1 \\ T = 1 \quad , \qquad\qquad at \quad r = r_2 \\ e_1 \dfrac{\partial^3 \eta}{\partial z^3} + e_2 \dfrac{\partial^3 \eta}{\partial z \partial t^2} + e_3 \dfrac{\partial^2 \eta}{\partial z \partial t} = -R_e \delta_{\circ}\left(\dfrac{\partial w}{\partial t} + u\dfrac{\partial w}{\partial r} + w\dfrac{\partial w}{\partial z}\right) + \\ \quad + \dfrac{1}{r}\dfrac{\partial}{\partial r}(rS_{rz}) + \delta_{\circ}\dfrac{\partial S_{zz}}{\partial z} \\ \quad + G_r T \; at \; \eta = r = r_i, i = 1,2 \end{array}\right\}, \qquad (14)$$

where $R_e = \dfrac{ca\rho}{\mu_{\circ}}$ is the Reynolds number, $G_r = \dfrac{\rho g \beta_T (T_{\circ} - T_1)a^2}{\mu_{\circ}c}$ is the Grashof number, $P_r = \dfrac{\mu_{\circ}c_p}{k_{\circ}}$ is the Prandtl number, $S_c = \dfrac{v_{\circ}}{D_{\circ}}$ is the Schmidt number, $E_c = \dfrac{v_{\circ}^2}{c_p(T_{\circ} - T_1)}$ is the Eckert number, $E_1 = -\dfrac{\tau_1}{\lambda^3}, E_2 = \dfrac{m_1 c^2}{\lambda^3}, E_3 = \dfrac{dc}{\lambda^2}$ are the non-dimensionless wall compliant parameters. The components of non-dimensional stresses for Jeffery fluid are evaluated as

$$\left.\begin{array}{l} S_{rr} = \dfrac{2\delta_{\circ}\mu(T)}{1+\lambda_1}\left[1 + \dfrac{\delta_{\circ}\lambda_2 c}{a}\left(\dfrac{\partial}{\partial t} + u\dfrac{\partial}{\partial r} + w\dfrac{\partial}{\partial z}\right)\right]\dfrac{\partial u}{\partial r}, \\ S_{rz} = -\dfrac{\mu(T)}{1+\lambda_1}\left[1 + \dfrac{\delta_{\circ}\lambda_2 c}{a}\left(\dfrac{\partial}{\partial t} + u\dfrac{\partial}{\partial r} + w\dfrac{\partial}{\partial z}\right)\right]\left(\delta_{\circ}\dfrac{\partial u}{\partial z} + \dfrac{\partial w}{\partial r}\right), \\ S_{\theta\theta} = \dfrac{2\delta_{\circ}\mu(T)}{1+\lambda_1}\left[1 + \dfrac{\delta_{\circ}\lambda_2 c}{a}\left(\dfrac{\partial}{\partial t} + u\dfrac{\partial}{\partial r} + w\dfrac{\partial}{\partial z}\right)\right]\dfrac{u}{r}, \\ S_{zz} = \dfrac{2\delta_{\circ}\mu(T)}{1+\lambda_1}\left[1 + \dfrac{\delta_{\circ}\lambda_2 c}{a}\left(\dfrac{\partial}{\partial t} + u\dfrac{\partial}{\partial r} + w\dfrac{\partial}{\partial z}\right)\right]\dfrac{\partial w}{\partial z} \end{array}\right\} \qquad (15)$$

For the present analysis, we assume that dynamic viscosity μ, the thermal conductivity K [24-30]

$$\left.\begin{array}{l} \mu(T) = e^{-a_1 T} = 1 - a \; T + \dfrac{a^2 T^2}{2!} - \dfrac{a^3 T^3}{3!}...., \\ K(T) = 1 + b_1(T_{\circ} - T_1) T = 1 + b\theta_f, \end{array}\right\} \qquad (16)$$

3. Semi-Anaytical Hpm Solutions

In order to solve the nonlinear boundary value problem described by eqns. (10) –(13) under boundary conditions (14) under the long wavelength approximation $\delta_0 \rightarrow 0$. Utilizing eqns. (16), we construct the following homotopy, employing the **HPM** approach [47,48]:

$$(1-q)(L_1(W) - L_1(W^0)) + q\left[\frac{\partial}{\partial r}\left\{\frac{1}{r}\frac{\partial}{\partial r}\left(\frac{r\,\mu(T)}{1+\lambda_1}\frac{\partial W}{\partial r}\right)\right\} + G_T\frac{\partial \theta_f}{\partial r}\right] = 0, \qquad (17)$$

$$(1-q)\left(L_2(\theta_f) - L_2(\theta_f^0)\right) + q\left[\frac{1}{r}\frac{\partial}{\partial r}\left(r\,K(T)\frac{\partial \theta_f}{\partial r}\right) + E_C P_r\left(\frac{\mu(T)}{1+\lambda_1}\left(\frac{\partial W}{\partial r}\right)^2\right)\right] = 0, \quad (18)$$

The forms of the solutions of the equations (17-18) are as follows

$$\left.\begin{array}{l}W(r,z,t) = \sum q^n\, W_n(r,z,t),\\[2mm] \theta_f(x,y,t) = \sum q^n\, \theta_{f_n}(r,z,t),\end{array}\right\} \qquad (19)$$

Where q $\in$ [0,1] is an embedding parameter, $L_1 = \frac{\partial}{\partial r}\left(\frac{1}{r}\frac{\partial}{\partial r}\left(r\frac{\partial}{\partial r}\right)\right)$, $L_2 = \frac{1}{r}\frac{\partial}{\partial r}\left(r\frac{\partial}{\partial r}\right)$. let us suggest the initial guess

$$W_0 = \frac{1+\lambda_1}{\gamma(2-\beta)}r^{3-\beta}F[z,t] - g_1[r] - \frac{\alpha_1}{\beta}r^{-\beta} + \alpha_2, \qquad (20)$$

$$\theta_f^0 = \frac{\text{Log}[r_1] - \text{Log}[r]}{\text{Log}[r_1] - \text{Log}[r_2]}, \qquad (21)$$

Where

$$g_1[r] = \frac{r^{2-\beta}\gamma(4-\beta+2(-2+\beta)\text{Log}[r] - 2(-2+\beta)\text{Log}[r_1])G_T}{4(-2+\beta)^2(\text{Log}[r_1] - \text{Log}[r_2])(1+\lambda_1)}, \qquad (22)$$

$$\alpha_1 = -\frac{1}{-r_1^{-\beta}+r_2^{-\beta}}\left(-1 + \frac{(-4+\beta)\gamma\,G_T\,r_1^{2-\beta}}{4(-2+\beta)^2(\text{Log}[r_1] - \text{Log}[r_2])(1+\lambda_1)}\right.$$
$$-\frac{\gamma(-4+\beta+2(-2+\beta)\text{Log}[r_1] - 2(-2+\beta)\text{Log}[r_2])G_T r_2^{2-\beta}}{4(-2+\beta)^2(\text{Log}[r_1] - \text{Log}[r_2])(1+\lambda_1)} + \frac{\delta\,r_1^{2-\beta}(1+\lambda_1)}{(-2+\beta)\gamma}$$
$$\left.-\frac{(1+\phi\text{Cos}[2\pi(-t+z)])r_2^{2-\beta}(1+\lambda_1)}{(-2+\beta)\gamma}\right), \qquad (23)$$

$$\alpha_2 = -\frac{1}{-r_1^{-\beta}+r_2^{-\beta}}\left(-1 + \frac{(-4+\beta)\gamma G_T\,r_1^{2-\beta}}{4(-2+\beta)^2(\text{Log}[r_1] - \text{Log}[r_2])(1+\lambda_1)}\right.$$
$$-\frac{\gamma(-4+\beta+2(-2+\beta)\text{Log}[r_1] - 2(-2+\beta)\text{Log}[r_2])\,G_T\,r_2^{2-\beta}}{4(-2+\beta)^2(\text{Log}[r_1] - \text{Log}[r_2])(1+\lambda_1)} + \frac{\delta r_1^{2-\beta}(1+\lambda_1)}{(-2+\beta)\gamma}$$
$$\left.-\frac{(1+\phi\text{Cos}[2\pi(-t+z)])r_2^{2-\beta}(1+\lambda_1)}{(-2+\beta)\gamma}\right), \qquad (24)$$

$$\gamma = r_1^{-\beta}, \beta = \frac{a}{\text{Log}[r_1] - \text{Log}[r_2]}, \qquad (25)$$

$$F[z,t] = e_1\frac{\partial^3\eta(z,t)}{\partial z^3} + e_2\frac{\partial^3\eta(z,t)}{\partial z\partial t^2} + e_3\frac{\partial^2\eta(z,t)}{\partial z\partial t}, (26)$$

Substituting the solutions (20-21) into equations. (17-18), and equating the terms of the same power of q, by equating all terms of $q^2, q^3, ...$, we get the following system of ordinary differential equation

Zero Order System

$$\left.L_1(W_0) - L_1(W^0) = 0, \qquad L_2\left(\theta_{f_0}\right) - L_2(\theta_f^0) = 0,\right\} \qquad (27)$$

With the following boundary conditions

$$\left.\begin{array}{ll}W_0 = 0, \quad \theta_{f_0} = 0, & at\ r = r_1,\\[2mm] \theta_{f_0} = 1, & at\ r = r_2,\\[2mm] e_1\frac{\partial^3\eta}{\partial z^3} + e_2\frac{\partial^3\eta}{\partial z\partial t^2} + e_3\frac{\partial^3\eta}{\partial z\partial t} = \frac{1}{r}\frac{\partial}{\partial r}\left(\frac{re^{-a\,\theta_{f_0}}}{1+\lambda_1}\frac{\partial W_0}{\partial r}\right) + G_T\,\theta_{f_0},\\[2mm] at\ \eta = r = r_i, \quad i = 1,2\end{array}\right\} \qquad (28)$$

The solutions of the above zero order systems can be obtained by using equations (20-21) , as following

$$
\left.\begin{array}{c}
W_0 = \dfrac{1+\lambda_1}{\gamma(2-\beta)} r^{3-\beta} F[z,t] - g_1[r] - \dfrac{\alpha_1}{\beta} r^{-\beta} + \alpha_2, \\[2mm]
\Theta_{f_0} = \dfrac{Log[r_1] - Log[r]}{Log[r_1] - Log[r_2]},
\end{array}\right\} \qquad (29)
$$

First Order System

$$
\left.\begin{array}{l}
L_1(W_1) = -\dfrac{\partial}{\partial r}\left(\dfrac{1}{r}\dfrac{\partial}{\partial r}\left(\dfrac{r(e^{-a\,\Theta_{f_0}})}{1+\lambda_1}\dfrac{\partial W_0}{\partial r}\right)\right) - G_T \dfrac{\partial \Theta_{f_0}}{\partial r}, \\[4mm]
L_2\left(\Theta_{f_1}\right) = -\dfrac{1}{r}\dfrac{\partial}{\partial r}\left(r\left(1+b\,\Theta_{f_0}\right)\dfrac{\partial \Theta_{f_0}}{\partial r}\right) - E_C P_r \left(\dfrac{e^{-a\,\Theta_{f_0}}}{1+\lambda_1}\left(\dfrac{\partial W_0}{\partial r}\right)^2\right)
\end{array}\right\} \qquad (30)
$$

With the following boundary conditions

$$
\left.\begin{array}{cc}
W_1 = 0, & at\ r = r_1, \\
\Theta_{f_1} = 0, & at\ r = r_i,\ i = 1,2 \\[2mm]
0 = \dfrac{1}{r}\dfrac{\partial}{\partial r}\left(\dfrac{r\left(-a\,\Theta_{f_0} + \dfrac{a^2}{3}\Theta_{f_0}\Theta_{f_1}\right)}{1+\lambda_1}\dfrac{\partial W_0}{\partial r} + \left(\dfrac{r\,e^{-a\,\Theta_{f_0}}}{1+\lambda_1}\dfrac{\partial W_1}{\partial r}\right)\right) + G_T \dfrac{\partial \Theta_{f_1}}{\partial r}, \\[4mm]
at\ r = r_i,\ i = 1,2
\end{array}\right\}, \qquad (31)
$$

The solution of the above first order system can be obtained by using equations (31) as following

$$
\left.\begin{array}{c}
W_1 = g_5[r] + \dfrac{\alpha_3}{4}r^2 + \alpha_4 Log[r] + \alpha_5, \\[2mm]
\Theta_{f_1} = g_\theta^2[r] + \alpha_7 Log[r] + \alpha_{8,}
\end{array}\right\}, \qquad (32)
$$

where,

$$
g_2^0[r] = -\dfrac{\partial}{\partial r}\left(\dfrac{1}{r}\dfrac{\partial}{\partial r}\left(\dfrac{r\,e^{-a\,\Theta_{f_0}}}{1+\lambda_1}\dfrac{\partial W_0}{\partial r}\right)\right) - G_T \dfrac{\partial \Theta_{f_0}}{\partial r}, \qquad (33)
$$

$$
g_2^1[r] = \dfrac{\partial}{\partial r}\left(\dfrac{1}{r}\dfrac{\partial}{\partial r}\left(\dfrac{r\left(-a\,\Theta_{f_0} + \dfrac{a^2}{3}\Theta_{f_0}\Theta_{f_1}\right)}{1+\lambda_1}\dfrac{\partial W_0}{\partial r}\right)\right)
$$

$$
+ G_T \dfrac{\partial \Theta_{f_1}}{\partial r}, \qquad (34)
$$

$$
g_3[r] = \int \dfrac{g_2^0[r]}{r}\,dr\,, g_4[r]
$$

$$
= \int r\,g_3[r]\,dr, g_5[r]
$$

$$
= \int \dfrac{g_4[r]}{r}\,dr\,, \qquad (35)
$$

$$
\alpha_3 = \dfrac{f_2[r_2]f_4[r_1] - f_2[r_1]f_4[r_2]}{f_3[r_1]f_4[r_2] - f_3[r_2]f_4[r_1]}, \alpha_4 = \dfrac{f_2[r_2]f_3[r_1] - f_2[r_1]f_3[r_2]}{f_3[r_2]f_4[r_1] - f_3[r_1]f_4[r_2]}, \qquad (36)
$$

$$
\alpha_5 = -\left(g_5[r_1] + \dfrac{\alpha_3}{4}r_1^2 + \alpha_4 Log[r_1]\right), f_1[r]
$$

$$
= \dfrac{e^{-a\,\Theta_{f_0}}}{1+\lambda_1}, \qquad (37)
$$

$$f_2[r] = g_4[r]\left(f_1[r] + r\frac{\partial f_1[r]}{\partial r}\right) + r\,g_2[r]$$
$$+ r\,f_1[r]\ \frac{\partial g_4[r]}{\partial r}, \tag{38}$$

$$f_3[r] = \frac{r}{2}\left(2\,rf_1[r] + \frac{\partial f_1[r]}{\partial r}\right),\ f_4[r] = f_1[r] + r\frac{\partial f_1[r]}{\partial r}, \tag{39}$$

$$g_\theta[r] = -\frac{1}{r}\frac{\partial}{\partial r}\left(r\left(1 + b\,\Theta_{f_0}\right)\frac{\partial\,\Theta_{f_0}}{\partial r}\right) - E_C P_r\left(\frac{e^{-a\,\Theta_{f_0}}}{1+\lambda_1}\left(\frac{\partial W_0}{\partial r}\right)^2\right), \tag{40}$$

$$g_\theta^1[r] = \int r g_\theta[r]\,dr,\quad g_\theta^2[r] = \int\frac{g_\theta^1[r]}{r}\,dr, \tag{41}$$

$$\alpha_7 = -\frac{g_\theta^2[r_1] - g_\theta^2[r_2]}{\text{Log}[r_1] - \text{Log}[r_2]},\ \alpha_8 = -\frac{-\text{Log}[r_2]g_\theta^2[r_1] + \text{Log}[r_1]g_\theta^2[r_2]}{\text{Log}[r_1] - \text{Log}[r_2]}, \tag{42}$$

Then the solutions of equations (17-18) according to the boundary equations (14), by using HPM can be written as follows;

$$\left.\begin{array}{c}w(x,y,t) = \lim_{q\to1} W(r,z,t)\ ,\\ T(r,z,t) = \lim_{q\to1}\Theta_f(r,z,t),\end{array}\right\}, \tag{43}$$

4. Results And Interpretation

Selected computations are presented in **Figs 2-12**. In all cases smooth and stable solutions have been obtained with **HPM.** Figs. 2-3 illustrate the dynamic viscosity, and thermal conductivity With an elapse in time, there is a significant depression in dynamic viscosity (fig. 2). Furthermore a steady ascent in viscosity accompanies a rise in value of the radius-however a critical value of radius is attained corresponding to the optimum viscosity attained. Viscosity peak is also observed to be displaced slightly to a higher radius with a *decrease* in time. Fig. 3 shows that thermal conductivity is reduced with both an increase in Prandtl number and Eckert number. Thermal conductivity is also maximized at radius values of approximately 60 (as with viscosity). However profiles become increasingly skewed to the right with lower Prandtl numbers.

The increased time for relaxation of the fluid leads to a depression in viscosity. This trend has also been identified in a number of other studies including Nadeem and Akbar [23]. In rheology [7] the reduced viscosity has also been associated with a drop in tensile stresses in the viscoelastic fluid with progression in time, which aids relaxation of the liquid and contributes to a decrease in bulk viscosity of the fluid. It would appear that the Jefferys viscoelastic model also obeys this physical characteristic. Even though relatively small time elapses have been considered in fig. 2, the results seem promising for transport of rheological liquids, in particular for biochemical waste peristaltic pumps, where increased efficiency is achieved with lower viscosity, as elaborated by for example, Tripathi and Bég [21] for straight conduits and also earlier by Rath [32] for curved tube transport.

The reduction in viscosity will serve also to decrease the frictional resistance on the wall interiors manifesting in enhanced pumping efficiencies. The computations in fig. 2 correspond to a non-zero curvature and this shows that peristaltic efficiency can be enhanced in curved systems. The physical interpretation for the decrease in thermal conductivity with increasing Prandtl number (*Pr*) relates to the inverse relationship of these two variables. *Pr* is the ratio of the product of dynamic viscosity and specific heat capacity to the thermal conductivity. As Prandtl number increases, for a constant viscosity and specific heat capacity, the thermal conductivity must reduce. It also embodies the relative rate of viscous (momentum) diffusion to energy diffusion. The momentum diffusion rate will therefore increase, as the thermal (energy) diffusion rate falls. For *Pr* < 1, as investigated in fig. 3, the momentum diffusion rate is always lower than thermal diffusion rate. However the increase in Prandtl number elevates the magnitudes of the former with regard to the latter. The implication for actual peristaltic processes (e.g. gastric transport or industrial hot waste transport) is that less heat is diffused for higher Prandtl number suspensions. This will inevitably also influence the relative ease with which materials can be pumped in the configuration. Hotter fluids will slip with greater ease. The Eckert number (*Ec*) is also a key parameter which is associated with viscous heating i.e. kinetic energy dissipation and conversion to heat. As *Ec* is increased the kinetic energy converted to heat is enhanced. Great heat has therefore to be transported in the regime and this will depress thermal conductivity, as observed in fig. 3.
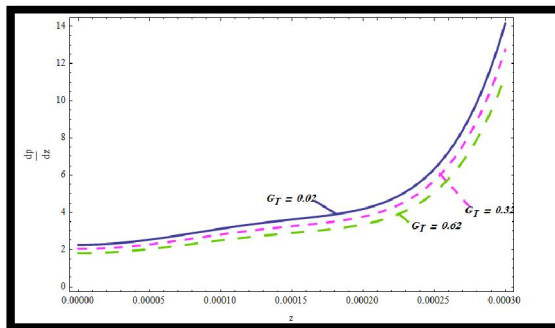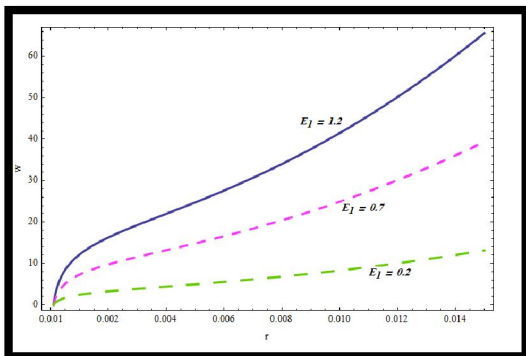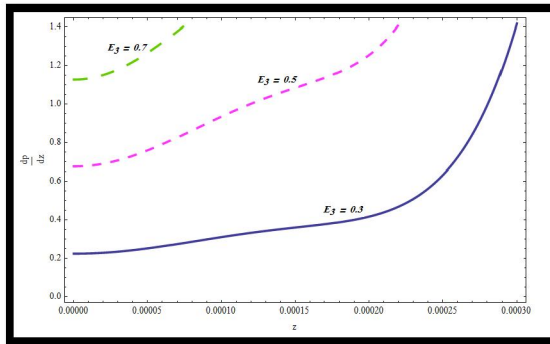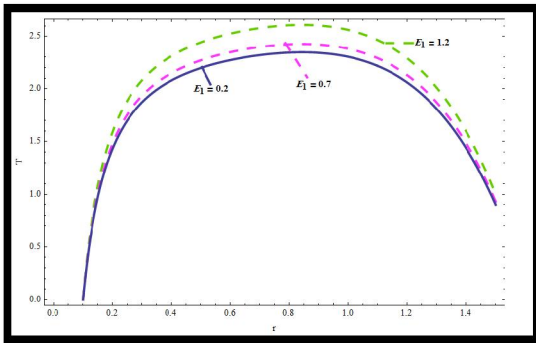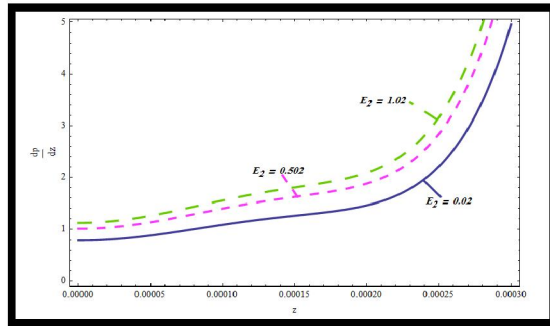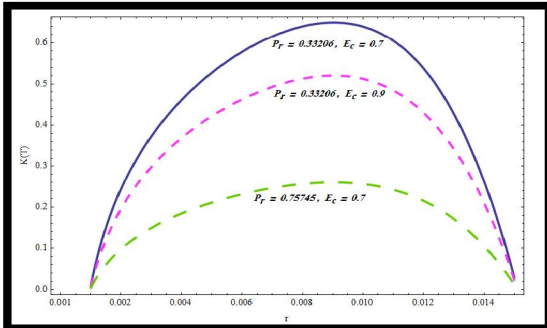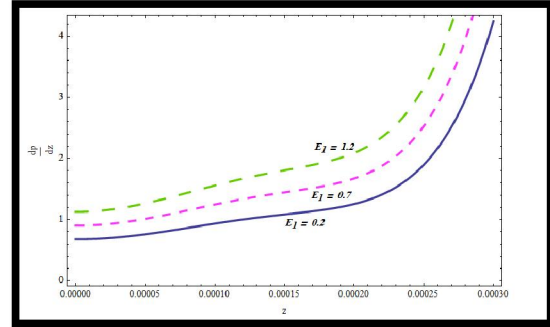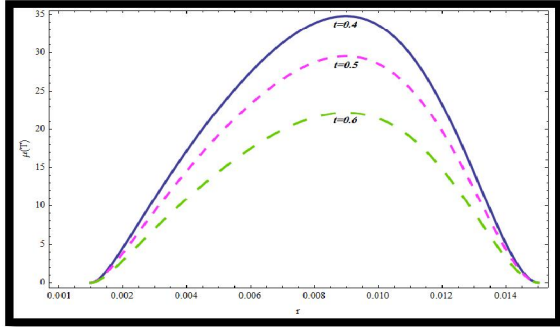
Figure (5). Velocity distribution **w** versus radius **r** for different values of wall compliant parameter.

Figure (9). Pressure gradient ($\frac{dp}{dz}$) versus **z** for different values of thermal Grashof number.

Figs 4, 5 depict the effect of the wall compliance parameter (E_1) on the temperature and axial velocity distributions in the regime, respectively, versus radial coordinate. This parameter, defined by $E_1 = -\dfrac{\tau_1}{\lambda^3}$ a arises in the elastic wall boundary conditions (16), and is a coefficient of a third order term, $\left\{ E_1 \dfrac{\partial^3 \eta}{\partial z^3} \right\}$ - as such it will exert a considerable influence on flow characteristics. With increasing E_1, temperature is accentuated in the regime significantly implying that with greater wall tension, the regime is heated more substantially. This is no doubt associated intimately with the acceleration in the axial flow which also accompanies an increase in the compliance parameter, E_1, as observed in fig. 6. Greater tension in the conduit wall clearly aids in momentum development and will also lead to an enhanced peristaltic pumping efficiency. Similar observations have been made by Alsaedi *et al.* [33] for Ostwald-deWaele shear-thinning fluids, Hina *et al.* [34] for Newtonian fluids and Ali *et al.* [35] for third grade viscoelastic fluids.

Fig. 6 presents the response in *axial* pressure gradient distribution to a variation in the first compliance parameter (E_1). With increasing axial coordinate i.e. longitudinal coordinate, the pressure gradient initially ascends smoothly, peaks and then decays at larger z values. As E_1 increases, the pressure gradient is clearly substantially elevated. This is physically with the axial acceleration computed earlier in fig. 5. Greater tension in the conduit walls will as elaborated earlier, act to accelerate the flow and enhance both axial velocity and pressure gradient. This will effectively boost the peristaltic pumping efficiency for the system. Although the latter has not been plotted, for brevity, the correlation between axial velocity, axial pressure gradient and hydromechanical efficiency is clearly documented in many studies including Stavitsky *et al.* [31], Tripathi *et al.* [13, 22], Bég *et al.* [14], Nadeem and Akbar [22] which have employed a diverse range of rheological models.

Fig. 7 illustrates the effect of the second wall compliance parameter, E_2 on axial pressure gradient. The pattern computed is very similar to fig. 8 i.e. a rise in the increase E_2 is observed to enhance the pressure gradient. E_2 arises also in the wall boundary conditions (16), but in a mixed derivative, viz, $\left\{ E_2 \dfrac{\partial^3 \eta}{\partial z \partial t^2} \right\}$ -it clearly influences the fluid dynamics as strongly as the first compliance parameter, E_1 and in fact generates considerably higher magnitudes of pressure gradient. E_2 is associated with the mass per unit area of the compliant wall, not the elastic tension. A denser wall constitution therefore also elevates pressure gradient.

Fig. 8 also shows that an increase in the third wall compliance parameter, E_3, results in a considerable elevation in axial pressure gradient. E_3 is connected to the viscous damping of the wall. Magnitudes of dp/dz are however a factor of 10 lower in fig. 10, than in fig. 9.

Fig.9 shows the thermal Grashof numbers (G_T the axial pressure distributions. A marked depression is caused in dp/dz both with increasing G_T value.

5. Conclusions

A **HPM** (homotopy perturbation method) semi-computational solution has been developed for nonlinear viscoelastic peristaltic flow, heat and mass transfer with cross-diffusion and viscous heating effects in an eccentric curved co-axial cylindrical conduit with compliant walls. The non-dimensionalized conservation equations have been solved. Variable fluid properties have also been incorporated for viscosity, thermal conductivity and mass diffusivity of the species (oxygen). Full details of **HPM** have been provided including selection of embedding parameters. The graphical solutions have shown that:

(i) Increasing thermal and solutal Grashof number strongly reduces axial pressure gradient at any value of radius.

(ii) An increase in the elastic (inertial), mass and viscous damping wall compliance parameters consistently enhance the axial pressure gradient.

(iii) Increasing elastic wall compliance parameter and solutal Grashof number respectively accelerate and decelerate the axial flow.

(iv) Increasing elastic wall compliance parameter enhances temperatures.

(v) Increasing time decreases dynamic viscosity of the Jefferys viscoelastic fluid.

(vi) Increasing Eckert number and Prandtl number both reduce the thermal conductivity of the viscoelastic fluid.

(vii) Increasing Soret number decreases species diffusivity whereas the converse response is computed with an increase in Eckert number.

The present study is relevant to gastric fluid mechanics and complex peristaltic pumps for biochemical waste conveyance. Although trapping and bolus formation have not been addressed in the present study these aspects are under investigation and will be described in an ensuing article.

Acknowledgments

grateful to the **late Prof. Dr. Hans J. Rath** (1947-2012), *Center of Applied Space Technology and Microgravity* (**ZARM**), University of Bremen, Germany, for some useful discussions in the spring of 2012 regarding applications of nonlinear peristaltic rheology in biochemical engineering.

References

1. R.K. Hobbie and B. Roth, *Intermediate Physics for Medicine and Biology*, Springer, New York, 4th edn (2007).
2. M.M. Rashidi, M. Keimanesh, O. Anwar Bég and T.K. Hung, Magnetohydrodynamic biorheological transport phenomena in a porous medium: A simulation of magnetic blood flow control and filtration, *Int. J. Num. Meth. Biomed. Eng.*, 27: 805–821, 2010
3. G.W. Scott Blair and D.C. Spanner, *An Introduction to Biorheology*, Elsevier Science Publishing Company, New York (1974).
4. H.L. Goldsmith, Biorheology in the 21st century, *Biorheology*, 49, 103-108 (2012).
5. A.C. Eringen, *Micro-continuum Field Theories-Vol II: Fluent Media*, Springer, New York (2001).
6. A.C. Eringen, Simple microfluids, *Int. J. Engineering Science*, 2, 205-217 (1964).
7. Juan de Vicente (Editor), *Viscoelasticity - From Theory to Biological Applications*, InTech, USA, (2012).
8. D.V. Davies and A J Palfrey, Viscoelastic properties of some pathological human synovial fluids, *Ann. Rheum. Dis.,* 28(2): 194-199 (1969).
9. G.B. Thurston and N.M. Henderson, Effects of flow geometry on blood viscoelasticity, *Biorheology*, 43(6), 729-46 (2006).
10. P. Sharif-Kashani, J-P. Hubschman, D. Sassoon and H. Pirouz Kavehpour, Rheology of the vitreous gel: Effects of macromolecule organization on the viscoelastic properties, *J. Biomechanics*, 44, 419–423 (2011).
11. H. C. Fu, C. W. Wolgemuth and T. R. Powers, Swimming speeds of filaments in nonlinearly viscoelastic fluids, *Phys. Fluids*, 21, 033102-1 - 033102-21 (2001).
12. D. Tripathi and O. Anwar Bég, A numerical study of oscillating peristaltic flow of generalized Maxwell viscoelastic fluids through a porous medium, *Transport in Porous Media*, 95, 337-348 (2013).
13. D. Tripathi, S.K. Pandey and O. Anwar Bég, Mathematical modelling of heat transfer effects on swallowing dynamics of viscoelastic food bolus through the human oesophagus, *Int. J. Thermal Sciences*, 70, 41-53 (2013).
14. O. Anwar Bég, M. Keimanesh, M. M. Rashidi and M. Davoodi, Multi-step DTM simulation of magneto-peristaltic flow of a conducting Williamson viscoelastic fluid, *Int. J. Appl. Math. Mech.*, 9 (6)1-19 (2013)
15. D. Tripathi, O. Anwar Bég and J.L. Curiel-Sosa, Peristaltic flow of generalized Oldroyd-B fluids with slip effects, *Computer Methods in Biomechanics Biomedical Engineering* (2012). DOI:10.1080/10255842.2012.688109
16. S. Hina, T. Hayat and A. Alsaedi, Heat and mass transfer effects on the peristaltic flow of Johnson-Segalman fluid in a curved channel with complaint walls, *Int. J. Heat Mass Tran.* 55, 3511-3521 (2012.)
17. O. Anwar Bég and D. Tripathi, Mathematica simulation of peristaltic pumping with double-diffusive convection in nanofluids: a bio-nanoengineering model, *Proc. IMechE. Part N: J. Nanoengineering and Nanosystems*, 225, 99-114 (2012).
18. J. G. Cuennet, A. E. Vasdekis, L. De Sio and D. Psaltis, Optofluidic modulator based on peristaltic nematogen microflows, *Nature Photonics,* 5, 234–238 (2011).
19. D. Tripathi and O. Anwar Bég, Magnetohydrodynamic peristaltic flow of a couple stress fluid through coaxial channels containing a porous medium, *J. Mechanics Medicine Biology*, 12 (5), 1250088.1-1250088.20 (2012).
20. D. Tripathi and O. Anwar Bég, Mathematical modeling of peristaltic pumping of viscoplastic fluids, *Proc. IMechE. Part H: J. Engineering in Medicine* (2013). *In press*
21. D. Tripathi, S.K. Pandey, A. Siddiqui and O. Anwar Bég, Non-steady peristaltic propulsion with exponential variable viscosity: A study of transport through the digestive system, Computer Methods Biomechanics and Biomedical Engineering, DOI.ORG/ 10.1080 / 10255842. 2012.703660 (2012).
22. S. Nadeem and N. Akbar, Peristaltic flow of a Jeffery fluid with variable viscosity in an asymmetric channel, *Zeitschrift fur Naturforschung*, 29, 713-722 (2009).
23. S. Nadeem and N. Akbar, Effects of heat transfer on Peristaltic transport of MHD Newtonian fluid with variable viscosity: Application of Adomian decomposition method, Comm. Nonlin. Sci. Num. Sim, 14, 3844-3855 (2009).
24. S. Nadeem and N. Akbar, Effects of temperature dependent viscosity on Peristaltic flow of a Jeffery-six constant fluid in a non-uniform vertical tube, *Comm. Nonlin. Sci. Num. Sim.* 15, 3950-3964 (2010).
25. S. Nadeem, Noreen Sher Akbar and M. Hameed, Peristaltic transport and heat transfer of a MHD

Newtonian fluid with variable viscosity, International Journal for Numerical Methods in Fluids, 63, 1375-1393 (2010).

26. S. Nadeem, Noreen Sher Akbar, Influence of temperature dependent viscosity on peristaltic transport of a Newtonian fluid: Application of an endoscope, Applied Mathematics and Computation 216, 3606-3619 (2010).

27. Nadeem, S., Akbar, N.S. and Hayat, T., Effects of variable viscosity on the peristaltic motion in a third order fluid, Zeitschrift fur Naturforschung A. 65a, 901 – 910 (2010).

28. S. Nadeem, Noreen Sher Akbar, Influence of heat transfer and variable viscosity in vertical porous annulus with peristalsis, Journal of porous media 14, 849-863 (2011).

29. Noreen Sher Akbar, S. Nadeem, Simulation of variable viscosity and Jeffrey fluid model for blood flow through a tapered artery with a stenosis Communications in Theoretical Physics, 57, 133-140 (2012).

30. S. Stavitsky, E.O. Macagno and J. Christensen, Finite element analysis of flow induced by contractions like those of the intestine, *J. Biomechanics*, 14, 183-193 (1981).

31. H.J. Rath, Peristaltic flow through a lobe-shaped tube, *Int. J. Mech. Sci.*, 24, 359-267 (1982).

32. A. Alsaedi, T. Hayat, M. Mustafa and S. Hina, Peristaltic flow of a pseudoplastic fluid in curved channel with wall properties, *ASME J Appl. Mechanics*, 80 (2) 024501 (7p) (2013).

33. S. Hina, T. Hayat, S. Asghar and A. A. Hendi, Influence of compliant walls on peristaltic motion with heat/mass transfer and chemical reaction, *Int. J. Heat Mass Transfer* 55, 3386-3394 (2012).

34. N. Ali, M. Sajid, Z. Abbas, T. Javed, Non-Newtonian fluid flow induced by peristaltic waves in a curved channel, *Eur. J. Mech.-B: Fluids*, 29,. 387–394 (2010).

35. N. Ali, M. Sajid, T. Javed, Z. Abbas, An analysis of peristaltic flow of a micropolar fluid in a curved channel, *Chin. Phys. Letts.*, 28, 1 014704 (4pp) (2011).

36. A. K. Yazdanpanh-Ardakani and H. Niroomand-Oscuii, New (ADINA-FSI) approach in modeling peristaltic transport of non-Newtonian fluid, *J. Mech. Med. Biol.* (2013). DOI: 10.1142/S0219519 4 1 3 5 00528.

37. C. R de Lima *et al.,* A biomimetic piezoelectric pump: computational and experimental characterization, *Sensors and Actuators A: Physical*, 152, 110-118 (2009).

38. S. Selvarajan, E.G. Tulapurkarab and V. Vasanta Ramc, A numerical study of flow through wavy-walled channels, *Int. J. Num. Meth. Fluids,* 26, 519-531 (1998).

39. R. Bhargava, S. Sharma, H.S. Takhar, T.A. Bég, O. Anwar Bég and T.K. Hung, Peristaltic pumping of micropolar fluid in porous channel- a model for stenosed arteries, *J. Biomech.*, 39, 649-669 (2006).

40. B.V.Rathish Kumar and K.B. Naidu, A numerical study of peristaltic flows, *Comp. Fluids*, 24, 161-176 (1995).

41. A. Ebaid, A new numerical solution for the MHD peristaltic flow of a bio-fluid with variable viscosity in a circular cylindrical tube via Adomian decomposition method, *Phys. Letters-A*, 372, 5321-5328 (2008).

42. K. Connington, Q. Kang, H. Viswanathan, A. Abdel-Fattah and S. Chen, Peristaltic particle transport using the lattice Boltzmann method, *Phys. Fluids*, 21, 053301 (2009).

43. H. Kozu, I. Kobayashi, M. Nakajima, K. Uemura, Analysis of flow phenomena in gastric contents induced by human gastric peristalsis using CFD, *Food Biophysics*, 5, 330-336 (2010).

44. J.H. He, Homotopy perturbation technique, *Computer Methods in Applied Mechanics and Engineering*, 178, 257–262 (1999).

45. A. B. Parsa, M. M. Rashidi, O. Anwar Bég and S. Sadri, Semi-computational simulation of magneto-hemodynamic flow in a semi-porous channel using optimal homotopy and differential transform method, *Comp. Biol. Med.* (2013). http://dx.doi.org/ 10.1016/j.compbiomed.2013.05.019i

46. A. F. Elsayed, Comparison between variational iteration method and homotopy perturbation method for thermal diffusion and diffusion thermo effects of thixotropic fluid through biological tissues with laser radiation existence, *Appl. Math. Model.*, 37, 3660–3673 (2013) .

47. D. Tripathi and O. Anwar Bég, Homotopy perturbation simulation of nonlinear peristaltic transport phenomena in viscoelastic-saturated porous media conduits, *Math. Biosci.,* (2013). In Press.

48. J. Biazar and H. Ghazvini. "Convergence of the homotopy perturbation method for partial differential equations" Nonlinear Analysis: Real World Applications 10 2633-2640 (2009).

4/15/2014